J. Fluid Mech. (1978), *vol.* 88, *part* 4, *pp.* 623–639
Printed in Great Britain

On internal gravity waves in an accelerating shear flow

By S. A. THORPE

Institute of Oceanographic Sciences, Wormley, Godalming, Surrey, England

(Received 31 December 1977)

The investigation of the effects which a changing mean flow has on a uniform train of internal gravity waves (Thorpe 1978*a*) is continued by considering waves in a uniformly accelerating stratified plane Couette flow with constant density gradient. Experiments reveal a change in the mode structure and phase distribution of the waves, and their eventual breaking near the boundary where the mean flow is greatest, the phase speed of the waves being positive. A linear numerical model is devised which accurately describes the waves up to the onset of their breaking, and this is used to investigate their energetics. The working of the Reynolds stress against the mean velocity gradient results in a very rapid transfer of energy from the waves to the mean flow, so that by the time breaking occurs only a small fraction of their initial energy remains for possible transfer into potential energy of the fluid.

The consequences have important applications in oceanography and meteorology, to flow stability and flow generation, and explain some earlier laboratory observations.

1. Introduction

This paper is concerned with the interactions between a changing mean flow and a train of internal gravity waves. It is known that, in the ocean, although internal gravity waves dominate the energy spectrum in a band between the inertial and Brunt–Väisälä frequencies, most of the energy resides in lower frequency motions. It is inevitable that the internal waves will be subjected to a changing 'mean' flow, i.e. they will encounter motions of much lower frequency with which they may interact.

The interactions between waves and mean flow may have important consequences. For example Holton & Lindzen (1972; see also Plumb 1977) have suggested that the quasi-biennial oscillation of the zonal wind in the tropical stratosphere arises from an interaction between the mean wind and large-scale equatorial waves.

An example of wave/mean-flow interaction in the ocean was described by Thorpe (1978*a*, hereafter referred to as I). Observations by Halpern (1974) show that when the upper layers of the ocean are accelerated by a wind stress, the Richardson number in the thermocline becomes small. The difference in the speed of the flow above and below the thermocline becomes comparable with the speed at which internal waves propagate, and they are prone to distortion and breaking. Some of these effects were examined in an experiment described in I in which internal waves were generated in a long closed tube containing two layers of liquid of different densities with a diffuse interface between them. The tube was tilted to initiate a uniformly accelerating mean flow. The waves were seen to distort and break, and an explanation was offered in terms of a finite amplitude description of waves in a steady flow. The energy exchanges involved were not discussed in I and effects of the mean flow acceleration were ignored

on the assumption that the motion was at any time 'quasi-steady'. These omissions are rectified here. The results show that very strong interactions take place between the wave and the changing mean flow. These lead to a rapid loss of wave energy through the working of the Reynolds stress on the mean velocity gradient and a corresponding increase in the kinetic energy of the mean flow, so that by the time breaking occurs (affecting now the potential energy of the mean flow) only a small fraction of the initial wave energy remains available for transfer.

We have made some more experiments which demonstrate these effects, using a fluid of constant density gradient rather than the 'almost two-layer' fluid of I. When the tube is tilted an accelerating flow with a nearly uniform velocity gradient, a stratified plane Couette flow, is produced, in which the Richardson number falls as $(\text{time})^{-2}$. The steady Couette flow is stable at all positive Richardson numbers, and it appears probable that the accelerating flow is also stable (in the sense that no infinitesimal disturbances grow indefinitely; see appendix). If, however, the flow initially contains a wave of small, but finite, amplitude the wave will ultimately break when the flow reaches some Richardson number which is a function of the wave slope and (non-dimensional) wavenumber. This may in practice limit attempts to generate such low Richardson number flows since some background wave noise is inevitable.

The properties of internal waves in a steady stratified plane Couette flow are reviewed in § 2 and the experiments are described in § 3. They demonstrate how the wave disturbance becomes concentrated at the boundaries of the gradient region, the vertical direction of energy transfer being determined by the sign of the vector–scalar product $\mathbf{c}.\mathbf{g}\times\boldsymbol{\Omega}$, where $\mathbf{c}$ is the wave speed (measured in a frame of reference in which the integrated mean flow is zero), $\mathbf{g}$ is the acceleration due to gravity and $\boldsymbol{\Omega}$ the vorticity in the mean flow. Such a redistribution may, in the ocean, lead to energy concentration at the top and bottom of the seasonal thermocline or perhaps in the benthic boundary layer.

A numerical experiment is described in § 4 and compared with the laboratory observations, and possible applications are discussed in the final section.

2. Finite amplitude internal gravity waves in a steady stratified plane Couette flow

As a preliminary to the experiments, we here present results for internal waves in a steady flow with constant velocity gradient U' and constant Brunt–Väisälä frequency N.

A finite amplitude theory for steady waves in a shear flow is given in I. The method used is a conventional one in which it is assumed that an ordered expansion of the flow variables in terms of a Fourier series can be made about a linear wave solution. The coefficients at successive orders are determined from the equations which result when the expressions for the flow quantities are substituted into the equation of motion and the Boussinesq approximation is made. It is plausible that such a method will give a good approximation for the wave as it approaches breaking (when the speed of particles somewhere in the flow becomes equal to the phase speed of the wave) at low Richardson numbers. Banks, Drazin & Zaturska (1976) have shown that, in a stably stratified shear flow with a simple maximum or minimum in the flow speed,

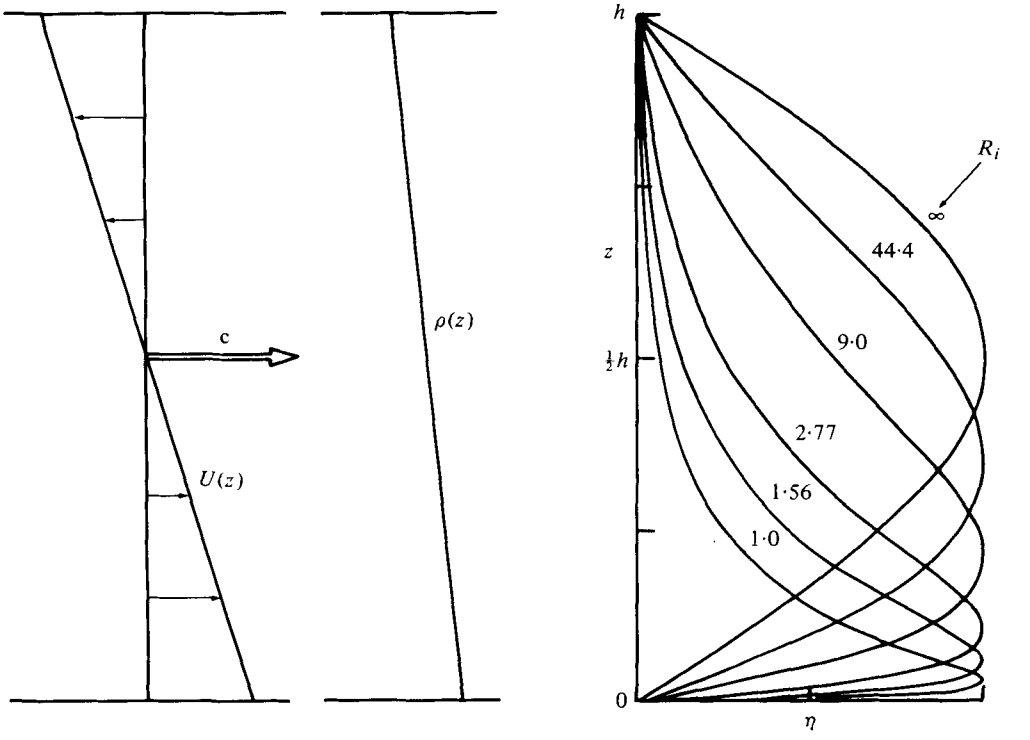

FIGURE 1. A sketch of the mean flow and density distribution and the vertical distribution of the amplitude of the linear solution for the first-order mode of wavelength $1{\cdot}97\,h$ (corresponding to experiment A) in steady flows at various Richardson numbers R_i.

there is a class of 'internal gravity waves modified by shear'. Waves of given mode and wavelength in this class have the property that their phase speed tends towards the maximum flow speed from above, or the minimum from below, as the Richardson number of the mean flow falls towards a critical value, which for some flows may be zero. As this critical value is approached, the flow needs less and less enhancement by the wave motion itself for the condition of breaking to be attained, and hence at low Richardson numbers an expansion about a linear wave solution appears appropriate. This solution corresponds to an eigenvalue of the Taylor–Goldstein equation

$$\left(\frac{d^2}{dz^2}+\frac{N^2}{(c-U)^2}-k^2+\frac{U''}{c-U}\right)\Psi = 0 \tag{1}$$

with $\Psi(0) = \Psi(h) = 0$. Here z is the vertical co-ordinate, $U(z)$ is the mean horizontal flow and c is the phase speed, found as an eigenvalue of the equation corresponding to waves of wavenumber k. When N and U' ($\equiv dU/dz$) are constant the solution may be expressed in terms of Bessel functions (Eliassen, Høiland & Riis 1953). For long waves the solution simplifies a little (Davey & Reid 1977), but it is still so complicated that, in proceeding to second and higher orders, product terms are encountered in the equations which render them beyond simple analytical solution. We have therefore proceeded as in I to a numerical solution.

We shall confine discussion to a particular case which corresponds to experiment A, which is described later. This experiment was fairly typical and illustrates the features we wish to discuss. Figure 1 shows a sketch of the mean flow and the (linear) first-order

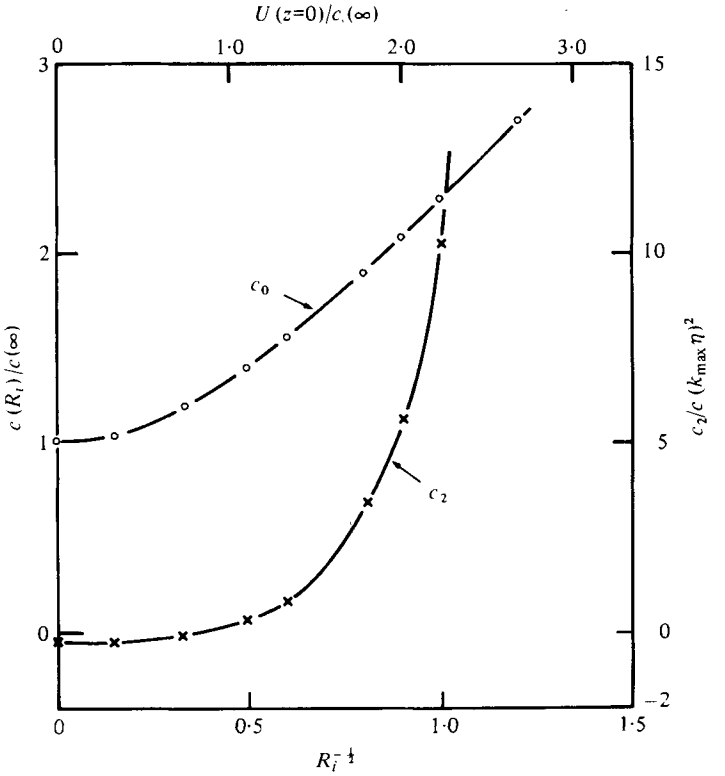

FIGURE 2. The variation of the phase speed c (normalized with the speed in the absence of mean flow $c(\infty)$) of the waves and the second-order correction to this speed, c_2 (normalized with c and the square of the maximum wave slope), with $R_i^{\frac{1}{2}}$ and $U(z=0)/c(\infty)$ for waves of length $1{\cdot}97\,h$ (corresponding to experiment A) in steady flows.

normalized wave amplitude $\eta = \Psi/(c-U)$ as a function of depth for a first-mode wave of length $1{\cdot}97\,h$ for various values of the Richardson number $R_i = N^2/U'^2$ of the mean flow. The effect of the flow is to displace the maximum elevation towards the lower boundary (U' is taken negative as shown in the sketch so as to correspond to the experiments), where the flow in the direction of the phase speed c is greatest. (U' positive would produce maximum elevation near the upper boundary.) Figure 2 shows the variation of c with $R_i^{-\frac{1}{2}}$ or with the speed at the lower boundary, to which c tends as R_i decreases as predicted by Banks *et al.* (1976). Figure 2 also shows the second-order correction to the phase speed, resulting from finite amplitude effects. This is negative for large R_i, but becomes positive and appears to become increasingly large as R_i decreases below unity. The solutions have not been continued to very small values of R_i because of difficulties in obtaining convergence and adequate resolution associated with the large displacements localized at the lower boundary.

Figure 3 shows the variation with $R_i^{-\frac{1}{2}}$ of the wave slope ($k \max \eta(z)$) at which the theory predicts that the horizontal particle speed somewhere in the wave becomes equal to the phase speed of the wave. Three curves are shown corresponding to the first-order (linear) solution and the second- and third-order solutions. These curves may be regarded as stability curves. Waves in a flow of given R_i with slope below the

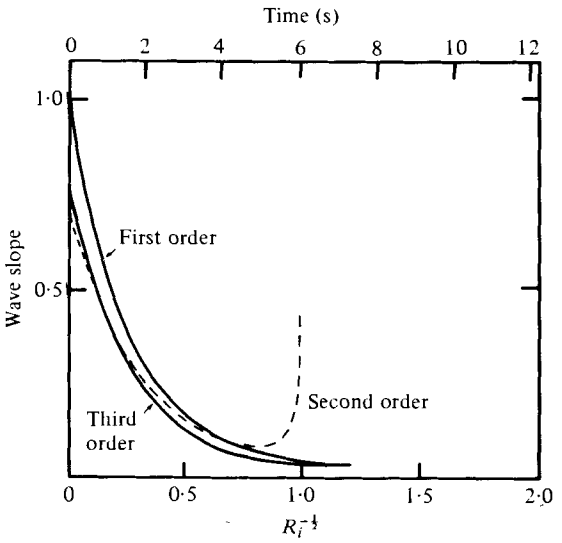

FIGURE 3. The slope of internal waves of the first mode and of length $1{\cdot}97\,h$ (corresponding to experiment A) required to generate horizontal velocities equal to the wave phase speed in steady flows at various $R_i^{-\frac{1}{2}}$. The upper horizontal scale shows the time at which the Richardson number in the lower scale is achieved in experiment A (see § 3).

curves are stable, but those with slopes greater than the 'critical slope' corresponding to points on the curve contain a region where the theory is strictly invalid, but in which it appears that the particles move forward more rapidly than the wave advances, so leading to gravitational instability, wave breaking and possibly rotor formation. The second-order phase speed increases with wave slope more rapidly than the second-order particle speed when R_i is less than about unity and hence, to second order, no waves, however large, are found which have particle speeds which are equal to the phase speed. This anomalous effect is however removed when the third-order terms are included. Except at large R_i the first- and third-order solutions fall close together. This does not however imply that the finite amplitude effects are negligible but rather that they are almost balanced, the increase in phase speed being comparable in size to the increase in particle speeds due to second- and third-order effects. Indeed, near the third-order 'critical slope' the second-order contributions to the wave amplitude become comparable to the first at $R_i \sim 1$, and for smaller R_i finite amplitude effects are important even at very small wave slopes.

The mean shear causes a considerable reduction in the wave slope necessary for incipient breaking. A mean flow Richardson number of unity reduces the third-order slope by a factor of about 19 from that in the absence of shear. Reductions of similar size have been found in numerical experiments with waves of other wavelengths, and in fluids of other density distributions (see I).

3. Laboratory experiments

The apparatus is a 4·85 m rectangular tube with Perspex side walls which is of height 16 cm and width 10 cm and which may be tilted about a horizontal axis normal to its length. At one end of the tube there is a flap wave maker (figure 4). When

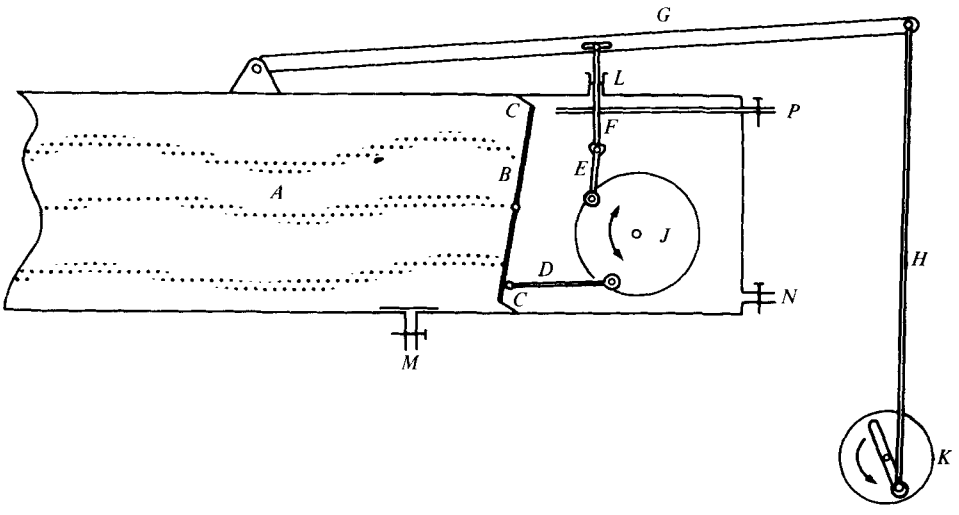

FIGURE 4. The wave maker. The waves in the brine solution A are generated by the oscillation of a vertical flap B about a horizontal axis. The flap is connected to the tube walls by a flexible rubber membrane C, and is driven through rods D, E, F, G, H, connecting linkages, and a disk J from an eccentric cam on disk K, itself driven from a motor through a continuously adjustable hydraulic gearbox. The entry to the liquid-filled tube is through an O-ring at L. The working section A and the volume containing the flap driving mechanisms D, J, E and F are filled simultaneously through inlet tubes M and N, air escaping from tube P until the drive volume is filled, when P is closed. The flap amplitude is controlled by adjusting the radial distance of the connexion H onto K.

operating at constant frequency this generates primarily the first-mode internal wave (Thorpe 1968*a*) when the tube is filled with a brine–water mixture of constant density gradient. A wave train is set up and, before reflexion has occurred at the far end of the tube, the tube is tilted to initiate a uniformly accelerating shear flow (Thorpe 1968*b*). (Some higher-order modes and harmonics are generated by the wave maker but these appear not to distort the wave form significantly in the centre of the tube provided that the tube is tilted soon after the waves are first generated, presumably because the higher modes and harmonics travel less rapidly than the first and are more rapidly dissipated by viscosity.)

The subsequent development of the waves in experiment *A* was photographed and is shown in figure 5 (plate 1). Dye has been added to the fluid during filling to mark layers of uniform density. The photographs show the wave form at approximately 2 s intervals, about half the period of the initial wave train. By only 2·1 s after the tube was tilted (figure 5*b*) it is clear that the wave phase is no longer constant through the depth of the tube, an observation of great importance since it suggests that, unlike waves in a steady flow (§ 2), these may support Reynolds stresses and energy may be transferred between the wave and the mean flow. We return to consider this in § 4.

The wave elevations become concentrated near the lower boundary as expected (figure 1) and at about 8 s after the tube was tilted the waves begin to break, fluid particles being carried forward more rapidly than the wave at their level can advance, and regions develop in which the fluid is gravitationally unstably stratified. Until the onset of wave breaking the maximum amplitude of the waves on the dyed layers remains roughly constant (see figure 8) and the maximum wave slope is about 0·089.

The steady flow stability diagram (figure 3) shows that, to third order, waves with this slope should break at $R_i = 2{\cdot}79$, which is reached at 3·7 s after the tube is tilted, much earlier than the time at which breaking is observed in the experimental accelerating flow.

The phase changes accompanying the evolution of the wave lead to the appearance of regions of much increased vertical density gradients, as well as regions (particularly those in which breaking develops) where the gradients are reduced. The use of shadowgraph imagery revealed regions of high density gradient advecting with the waves near the bottom boundary and first appearing at about $R_i = 1$. These regions were finely structured, suggesting the pattern of evolution of parasitic waves arising from parametric instability shown by McEwan & Robinson (1975), and there was some evidence of flow separation from the lower boundary, although whether this was the result of rotor formation or separation of the viscous sublayer is not clear.

Stronger evidence of rotor formation came from a study (experiment *B*) of the wave development after the tube had been returned to a horizontal position after being tilted for 5·5 s (figure 6, plate 2). Evolution of the wave continues for a while but the profile appears to tend towards a quasi-steady state (see also figure 12 and later discussion) having an asymmetrical wave form with a rounded front near the lower boundary, suggesting the presence of a rotor attached to the lower boundary.

It is unfortunate that this is a flow in which the largest velocities and most important wave phenomena are at or near the lower boundary, where viscous effects are most likely to be important. These were however almost excluded in a further experiment (experiment *C*, shown in figure 7, plate 3), made in a fluid stratified in three layers, with a linear density gradient in the middle layer between (and including) the upper and lower dye bands and uniform densities in the layers outside. This represents a case intermediate between the 'almost two-layer' experiments of I and the experiments with a constant density gradient described here. The experiment was conducted as before, the waves being generated first and the tube tilted to initiate a uniformly accelerating shear flow with a distribution of speed similar to the density profile. The development of the waves in the stratified central layer continues as already described, the disturbance vanishing from the upper dye layers and increasing in the lower, but with the maximum wave amplitude remaining almost constant. Breaking occurs at the lower edge of the stratified region, being preceded by a vertical asymmetry of the wave form and the suggestion of the influence of a second harmonic on the wave shape. Similar effects were observed and described in I. The phase differences observed in figure 5 are again visible and indicate an energy exchange with the mean flow, as we shall see in the next section.

4. Numerical studies of accelerating stratified flow

The appropriate linearized equations of motion for a fluid with constant N^2 are

$$\left(\frac{\partial}{\partial t} + U\frac{\partial}{\partial x}\right)\nabla^2\psi = g\frac{\partial \rho}{\partial x}\cos\alpha - g\frac{\partial \rho}{\partial z}\sin\alpha \quad \text{(vorticity)} \tag{2}$$

and

$$\left(\frac{\partial}{\partial t} + U\frac{\partial}{\partial x}\right)\rho = -\frac{N^2}{g}\frac{\partial \psi}{\partial x}, \tag{3}$$

where the density is $\rho_0(0)\,[(1-N^2z/g)+\rho]$, α is the angle of tilt of the tube,

$$U = N^2tz\sin\alpha$$

(Thorpe 1968*b*), ψ is the stream function, x is taken along the tube axis up the line of greatest slope and z is normal to x in the vertical plane. We look for a solution periodic in x of the non-dimensionalized form

$$\psi = (N^2/k)\,\phi(z,t)\exp ikx,$$

$$\rho = (N^2/gk)\,\rho(z,t)\exp ikx. \tag{4}$$

Writing $Z = kz$ and $\tau = Nt$, we have

$$(\partial/\partial\tau + i\tau Z\sin\alpha)\,\theta = (i\cos\alpha - \sin\alpha\,\partial/\partial Z)\,\rho, \tag{5}$$

and

$$(\partial/\partial\tau + i\tau Z\sin\alpha)\,\rho = -i\phi, \tag{6}$$

where

$$\theta = (\partial^2/\partial Z^2 - 1)\,\phi. \tag{7}$$

These equations are to be solved subject to the boundary conditions

$$\phi = \rho = 0 \quad \text{at} \quad Z = \pm\pi/2\beta,$$

with $\phi = \cos[(2n-1)\beta Z]\exp(-i\sigma\tau)$ and $\rho = \phi/\sigma$ for $\tau \leqslant 0$, where

$$\sigma^2 = [1+\beta^2(2n-1)^2]^{-1}$$

and n is an integer, corresponding to an initial free wave of mode n in the absence of a mean flow. Equations (5)–(7) are solved using a numerical finite-difference method. We write ρ, ϕ and θ as real and imaginary parts and use the finite-difference form of (6) (together with the initial conditions at the first step) to find ρ at $\tau+\Delta\tau$, where $\Delta\tau$ is the time step. Substitution of this solution for $\rho(Z, \tau+\Delta\tau)$ in (5) then determines $\theta(Z, \tau+\Delta\tau)$. Equation (7) is then solved by a shooting method with $\phi = 0$ at the lower boundary and with 200 steps ΔZ in the vertical to find a solution for ϕ which satisfies $\phi = 0$ at the upper boundary, thus advancing the whole solution by one time step. The numerical method was verified by running the program with $\alpha = 0$, giving a steady propagating wave, and ΔZ and $\Delta\tau$ were varied as a check on numerical convergence.

The solutions obtained have been plotted as lines of constant density at 2 s time intervals with the parameters adjusted to correspond to experiments *A* and *B*. These are shown in figures 5 and 6 respectively† alongside the photographs of the experiments at roughly corresponding times.

There is good agreement both in the form and phase of the waves in experiment *A* up to about 8 s, when imminent breaking is presumably accompanied by nonlinear effects not included in the numerical calculations. The vertical distribution of the wave amplitude η (determined using $\eta = g|\rho|/N^2$) is shown in figure 8 and fair agreement is found between the numerical calculation and laboratory experiment bearing in mind the difficulties of measuring the small displacements from the rather blurred edges of the dye lines. Comparison of these profiles with those corresponding to the

† A comparison may be made by making two transparencies of each figure and projecting these on an overhead projector with the numerical curves overlying the photographs between the arrows.

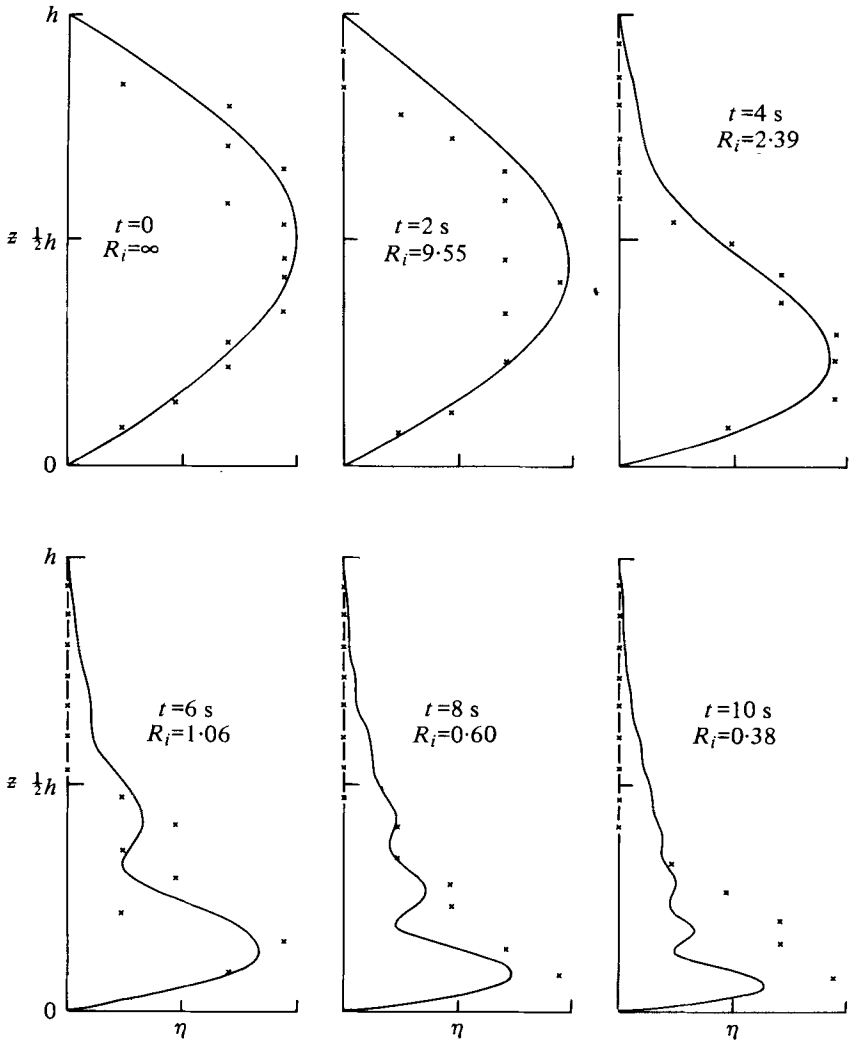

FIGURE 8. Profiles of the modulus of the vertical displacement η of lines of constant density in a first-mode wave in an accelerating flow. The parameters are chosen to correspond to experiment *A* at 2 s intervals. The initial amplitude is chosen to fit the maximum observed amplitude, which is used to normalize the curves. The points are measured from frames of a ciné film of the experiment at corresponding times (to within 0·04 s).

steady flow solutions (figure 1) shows that the level of the maximum displacement does not fall so rapidly as in the latter, and multiple peaks which have a downward phase velocity develop in the accelerating flow. These can also be seen in figure 5. It was at first thought that these might be a possible indication of instability of the accelerating flow (see appendix). It appears more likely, however, that they are associated with transient high-order modes arising largely from the mismatch between the developing wave form and the steady-state first-mode solution. The transients are less well developed and the form of η closer to the steady flow solution if a flow with the same Richardson number is developed at smaller values of α, i.e. if the acceleration is reduced.

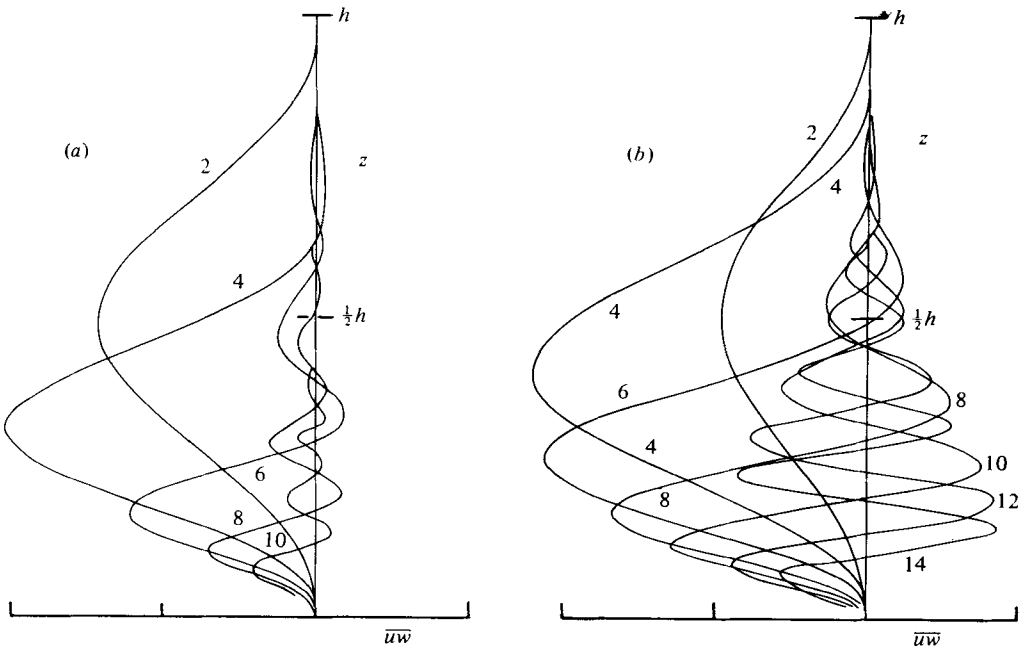

FIGURE 9. The mean values $\overline{uw}$, proportional to minus the Reynolds stress, plotted against depth and calculated at the times shown, with parameters chosen to correspond to (*a*) experiment *A* and (*b*) experiment *B*.

In view of the agreement between the numerical calculations and the experiments we feel some confidence in proceeding to examine the numerical solutions in more detail. One of the most important quantities of interest is the Reynolds stress $-\rho\overline{uw}$, where u and w are the horizontal and vertical components of velocity in the wave motion ($\partial\psi/\partial z$ and $-\partial\psi/\partial x$) and the bar denotes an average over one wavelength. The rate at which kinetic energy is transferred to the mean flow is $\overline{uw}U'$ (e.g. Phillips 1966, p. 200), which is positive if the Reynolds stress is positive since U' is negative. Figure 9 (*a*) shows the distribution of $\overline{uw}$ ($= -$ Reynolds stress) with depth at intervals of 2 s. It is structured, like η, but in the mean it is negative at all depths, showing that the waves lose energy to the mean flow. The time integral of the Reynolds stress up to 10 s has a form similar to η at 4 s, showing that the majority of the energy lost by the waves is transferred to the mean flow kinetic energy in the lower half of the tube.

Figure 10 (*a*) shows the variation of wave energy, plotted logarithmically, with time. Equipartition of energy is approximately maintained, but the wave loses about 82 % of its energy to the mean flow by 8 s *before* it begins to break. If all the potential energy of the wave was at this time transferred to the potential energy of the mean flow by wave breaking, whilst the remaining wave kinetic energy was transferred to the mean flow kinetic energy, the potential energy transfer divided by the kinetic energy transfer would be equal to 0·08, a figure reminiscent of the exchange fractions in Kelvin–Helmholtz instability or estimates of the flux Richardson number, to which it is related. If a smaller angle of tilt is used (figure 10*a*) and thus a less rapid acceleration of the mean flow, equipartition of energy is even more closely followed and the wave loses energy more rapidly in terms of the Richardson number of the accelerating mean flow.

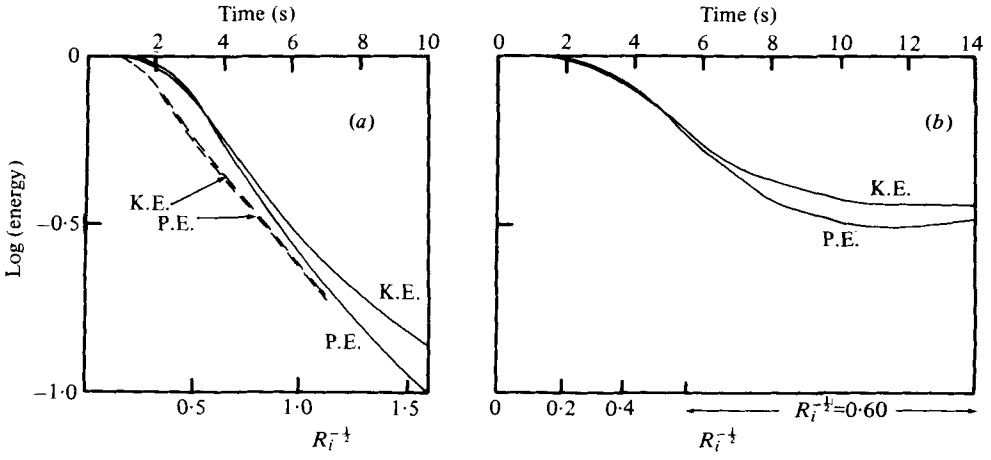

FIGURE 10. The logarithms of the potential (P.E.) and kinetic (K.E.) energy of the waves and their variation with time and $R_i^{-\frac{1}{2}}$. (*a*) Experiment *A*. The dashed lines show the logarithms of the energies calculated using an angle of tilt equal to half the angle used in the experiment and are correctly plotted against the $R_i^{-\frac{1}{2}}$ scale. (The equivalent time scale is twice that shown.) (*b*) Experiment *B*.

The justification for using figure 3 as a stability diagram for steady flow is that above the curves the particle speed appears to exceed the phase speed of the waves, thus leading, in a frame of reference moving with the waves, to a reversed flow and to S-shaped particle paths (which are also lines of constant density) and thus a region in which gravitational instability is possible. Such an argument is untenable in unsteady flows. Indeed there is evidence in the numerical experiments that the speeds of constant phase may for short times be less than the particle speeds in parts of the flow where no signs of breaking are observed in the experiments. We restrict attention however to the flow near the lower boundary, where the particle forward speed is greatest, and, for given wave slopes, calculate the times (or R_i) at which the numerical calculations predict that the forward speed first equals (and ever thereafter exceeds) the phase speed. The results are shown in figure 11. Although strictly the condition for breaking is invalid at the lower boundary, which is always a streamline, a local examination of the waves in a frame of reference moving with the accelerating flow a small distance above the boundary establishes curve (*a*) as a stability boundary in the same sense as before.

Also shown in figure 11 is the corresponding curve for half the angle of tilt (curve (*c*), plotted against R_i) and the first-order curve for steady flow from figure 3 (curve *b*). The effect of acceleration can be seen by comparing curves (*a*) and (*b*), and is to delay the onset of wave breaking. The curve for a smaller angle of tilt, and thus a smaller acceleration (curve *c*), follows more closely the steady flow.

Satisfactory comparison between the observations and the present theory is not possible for several reasons. The theory predicts breaking at the lower boundary, where it is indeed observed, but where viscosity locally modifies the flow. The numerical results are for a linear flow, and figure 3 strongly suggests that even in an accelerating flow nonlinear effects may be significant. The second- and third-order solutions for even the steady flow disregard the change in the mean flow profile which is produced

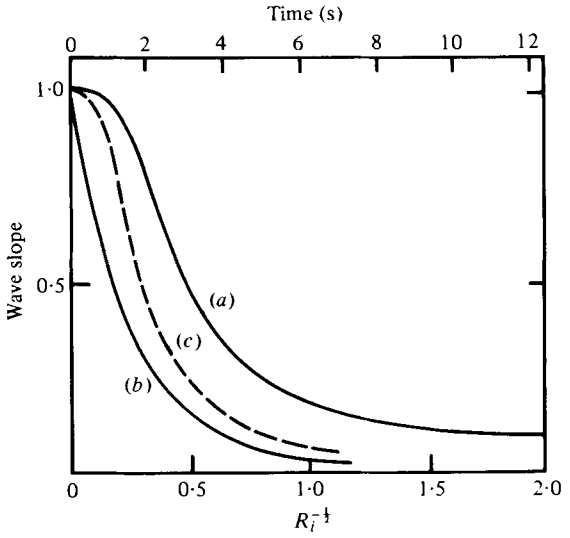

FIGURE 11. The 'stability diagram' calculated for experiment *A*. (*a*) Wave slope which, at any time (or at the corresponding mean flow Richardson number) in the accelerating flow, is just sufficient to promote currents which have a horizontal component equal to the phase speed of the waves near the lower boundary of the tube. (*b*) First-order curve of figure 3. (*c*) Curve corresponding to (*a*) but for a flow produced by tilting the tube through half the actual angle; this curve is correctly plotted against $R_i^{-\frac{1}{4}}$, but for it the time scale must be multiplied by 2.

by the energy transfer, and are therefore appropriate to a flow which differs slightly (but perhaps significantly) from that which is present in the tube at any R_i. The observed time and position of the breaking are however reasonably in accordance with the inferences of the theory.

Comparisons of the numerical results with experiment *B* are shown in figures 6, 12, 9(*b*) and 10(*b*). The wave amplitude profile η (figure 12) appears to tend towards the steady flow profile at the Richardson number of the flow, $R_i = 2{\cdot}77$, after the tube is returned to the horizontal at 5·5 s, but strong transients remain. The energy loss (figure 10*b*) resulting from the Reynolds stress (figure 9*b*) working on the main shear is seen to be permanent and there is a trend towards equipartition in the final flow. The 'critical' slopes at first, second and third order of waves in a steady shear flow at $R_i = 2{\cdot}77$ are found to be 0·109, 0·108 and 0·081 respectively, somewhat larger than the actual wave slope 0·066 but sufficiently close to suggest that a rotor may indeed have formed, particularly in view of the presence of transients which locally enhance the flow.

The density profile of experiment *C* was modelled by a hyperbolic-tangent profile which matched the gradients at the mid-depth and the numerical method was used to follow the development of a first-mode internal wave. (It was necessary to change the equations to account for the variable density gradient and corresponding accelerating mean flow, which introduces an additional term $-(\partial^2 U/\partial z^2)(\partial\psi/\partial x)$ on the left-hand side of (2), and to find the initial wave form by use of a separate program for waves in a steady flow of arbitrary density gradient; see Thorpe 1977.) Close comparison between the theory and experiment was not possible since too few density contours could be marked by dye (figure 7), but the general trends of the experiment,

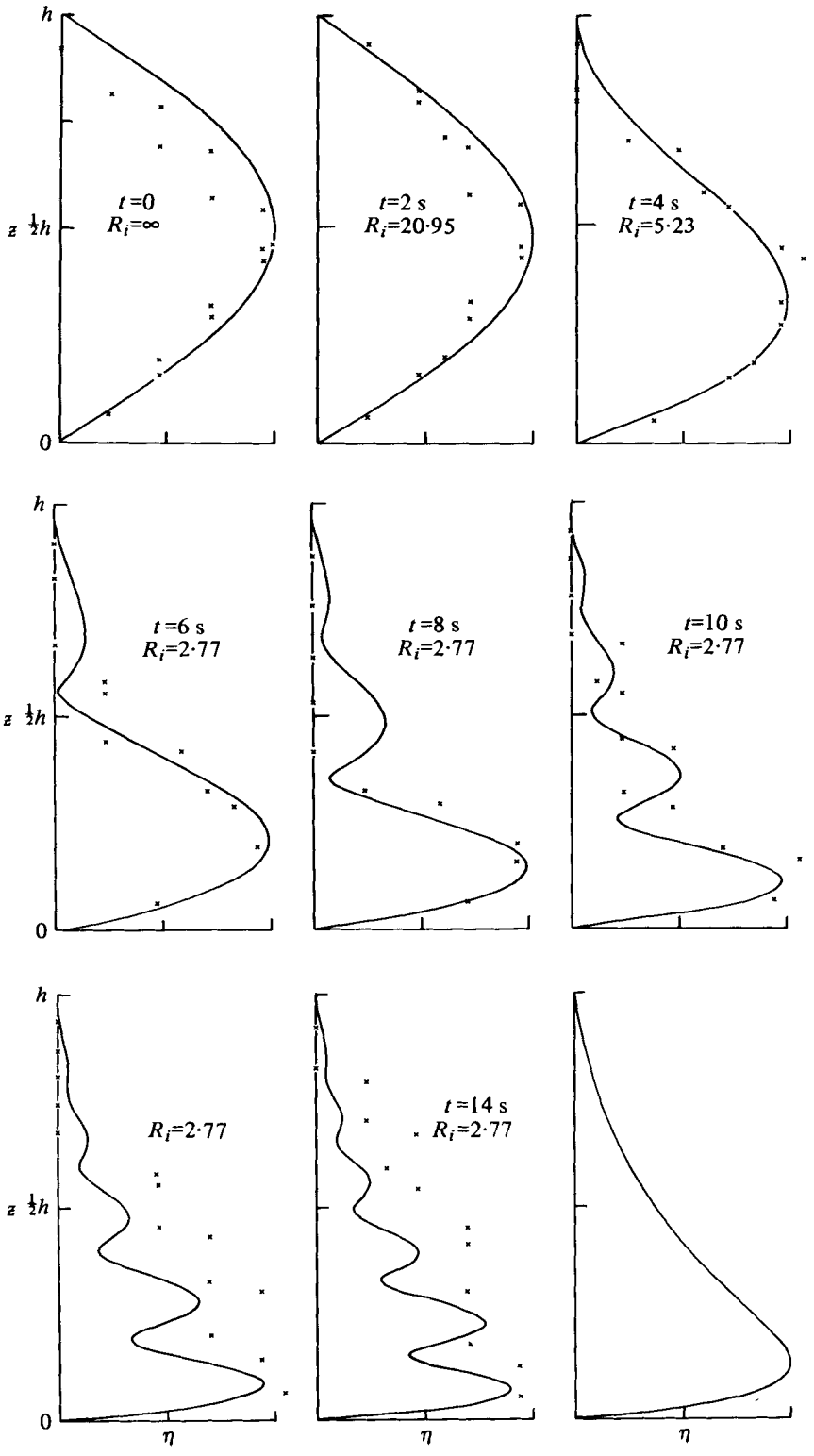

FIGURE 12. Profiles of the modulus of the vertical displacement η of lines of constant density in a first-mode wave in the flow of experiment B. The amplitude is initially normalized by the maximum amplitude observed in the experiment. The points are measured from a ciné film of the experiment at 2 s intervals up to 14 s. Also shown is the steady-flow linear solution η for waves of length $2{\cdot}53h$ in a flow with $R_s = 2{\cdot}77$, corresponding to the experiment.

the reduction in amplitude at the top and increase near the bottom of the stratified layer, as well as the small change in maximum amplitude, were demonstrated. At the time of wave breaking, 7 s after the tube was tilted, when the minimum Richardson number of the mean flow was 0·31, the numerical calculation showed that the total energy of the wave had been reduced to 0·33 of its initial value and that the potential energy was 1·9 times greater than the kinetic energy. In view of the nonlinear effects known here to be important in determining the wave shape (see I) further comparison with the linear theory is not attempted.

5. Discussion

5.1. *The stability of stratified shear flow*

We have here taken a view of flow stability different from that commonly adopted. We have looked, not at a small 'infinitesimal' disturbance to a given flow, but at a wave disturbance which is of finite amplitude (perhaps small but nevertheless finite and sometimes also nonlinear), and have determined whether the wave may develop a condition in which convective gravitational overturning is possible as the flow is accelerated. In practice such an examination is vital, for if a certain postulated flow is to be generated it will usually be via acceleration of the fluid. It may be impossible to produce the required flow if, in accelerating the fluid towards the desired flow state, waves which are inherent, if only as noise, become unstable, break and destroy the fluid density structure. Indeed curves such as those of figure 11 indicate that possibly, given some $\epsilon > 0$ however small, it may be impossible to reduce the Richardson number of certain flows (in fluids with given density and velocity profile shapes) by linear acceleration a ($= N^{-2}\,\partial^2 U/\partial t\,\partial z$) below a value $J(\epsilon, \lambda, a)$ in the presence of waves of non-dimensional length λ and slope ϵ, without upsetting the density structure. (Permanent destruction of the density profile must of course involve diffusive processes and neither these nor the effects of viscosity, which may ultimately be crucial, are considered here.) It may be that, for some slopes ϵ, J is greater than the critical value J_c of the Richardson number at which Kelvin–Helmholtz shear instability occurs in the mean steady flow. For example, in Couette flow with constant Brunt–Väisälä frequency, with which we have mostly been concerned here, $J_c = 0$, but the phase speed tends to the maximum flow speed as R_i tends to $\frac{1}{4}$ from above (Eliassen *et al.* 1953). Hence if the flow is quasi-steady $J(\epsilon, \lambda, 0) \geqslant \frac{1}{4} > J_c$, and any wave, however small, will become unstable and break when the mean flow has a Richardson number at which this mean flow is stable. Indications are that the wave solutions tend towards the steady solution as the flow acceleration is reduced. Hence although the Richardson number $J(\epsilon, \lambda, a)$ at which a wave in an accelerating flow becomes unstable will usually be less than $J(\epsilon, \lambda, 0)$ it may yet exceed J_c for sufficiently small accelerations. The wave may of course itself generate a shear sufficient to cause Kelvin–Helmholtz instability, but in some cases at least (see also I and the discussion there) wave 'breaking' will occur first. In none of the experiments has any sign been observed of the instabilities associated with curvature of the streamlines which were described by Scorer & Wilson (1963).

5.2. *Geophysical and other applications*

In I we pointed out the importance of internal wave breaking accompanying the acceleration of the upper layers of the ocean during periods of wind forcing. The novel aspect demonstrated here is the great importance and efficiency of Reynolds stresses, which transfer the wave energy into the mean motion very rapidly, leaving only a fraction of the initial wave energy available for transfer to potential energy when breaking occurs. We again recall the results of experiment *A*, in which over 80 % of the wave energy is lost in only two wave periods of the initial wave as the flow Richardson number is reduced to 0·6. This energy transfer accounts for the sudden collapse of the waves discussed in I after breaking. At this stage, although the wave amplitude is much the same as in the initial flow, the energy is much less and is concentrated near the breaking zone.

The energy remaining in the waves and potentially available for heat transfer by mixing is at the top or bottom of the shear layer depending on whether $\mathbf{c}$ (the vector phase speed), $\mathbf{g}$ and $\boldsymbol{\Omega}$ (the mean flow vorticity) form a right- or left-handed vector triad. This suggests that internal wave energy in the ocean may be redistributed by low-frequency changes, for example mesoscale eddies, and concentrated in those regions where the speed of the flow reaches a maximum, perhaps at the foot of the main thermocline or near-surface mixing layer in the ocean. The wave breaking which may result is a possible cause of temperature fine structure and perhaps explains the occurrence of persistent density inversions found at the foot of the seasonal thermocline in Loch Ness, where the mean Richardson number was between 1 and 10 (Thorpe 1978*b*). Similar wave breaking has been postulated at an atmospheric temperature inversion by Goodman & Miller (1977). It may be noted that the conditions of the experiments and those which appear to pertain to the upper ocean in periods of strong wind forcing, namely that the Richardson number is of order unity and the mean flow changes on a time scale comparable with the internal wave period, are not satisfied by the models usually adopted to describe the forcing of mean flow by waves (see for example Plumb 1977).

A mechanistic explanation of turbulent entrainment in a stratified fluid at high overall Richardson numbers is also suggested by the experiments. Let us consider a turbulent fluid layer driven by wind on its free upper surface or, as in Kato & Phillips' (1969) experiment, by a moving lid. The lower boundary, beyond which the fluid is in laminar flow, is stably stratified. Two sets of free internal gravity waves may be generated at the interface, one set with forward phase speeds moving in the direction of motion in the upper layer and the other set moving backwards. Waves with speeds lying between those of the two layers may possibly exist (see Banks *et al.*), but if so they are singular or neighbours to unstable modes and liable to lose energy rapidly. If the Richardson number is sufficiently high, however, no unstable modes can exist which will lead to a breakdown of the mean flow. Of the two sets of free waves, the forward moving are most likely to be generated since they have phase speeds most closely matched to the forcing turbulent fluctuations. These waves may grow under the action of the turbulent field, but will in any case transfer kinetic energy to the flow by Reynolds stresses in the mean velocity gradient. This transfer may eventually determine the mean flow velocity profile. If the waves grow sufficiently they will break sporadically *at the top* of the density interface (since $\mathbf{c}$, $\mathbf{g}$ and $\boldsymbol{\Omega}$ are a right-handed

triad), leading to the transfer of heat or solute into the turbulent region. The wave energy is provided by the turbulence and, as we have seen, of this only a small fraction is available for transfer to potential energy (or to transfer heat), the majority of the energy being transferred into the kinetic energy of the mean flow. These processes provide a mechanism for mixing which is absent in experiments on grid mixing with zero mean flow (see Turner 1973, chap. 9).

I am grateful for the assistance of Miss C. Barnes and Mr J. Herbert in preparing the experiments and measuring the films during their summer vacation from university.

Appendix. Waves in an unbounded uniformly accelerating stratified shear flow

We consider the development of waves which are of a scale much smaller than the dimensions of the experimental tube when the tube is tilted through an angle α.

The equation of motion is

$$\rho_0(0)\, D\mathbf{u}/Dt = -\nabla p - g\rho(\sin\alpha, 0, \cos\alpha), \tag{8}$$

where ρ is a specified function of z at $t = 0$. If initially $\rho = \rho_0(0)\,(1-\gamma z)$, then a solution with $u = 0$ at $t = 0$ is

$$u = g\gamma z t \sin\alpha, \quad \rho = \rho_0(0)\,(1-\gamma z)$$

(Thorpe 1968*b*). Consider now a small perturbation about this solution. Neglecting products of the perturbation terms and their derivatives, we can reduce (8) together with the continuity equation to one equation in the density perturbation ρ', where $\rho = \rho_0(0)\,(1-\gamma z) + \rho'$:

$$\left(\frac{\partial}{\partial t} + \beta z t \frac{\partial}{\partial x}\right)\left(\frac{\partial}{\partial t}\nabla^2 + \beta z t \frac{\partial}{\partial x}\nabla^2 + 2\beta t \frac{\partial^2}{\partial x\,\partial z}\right)\rho' = \beta \frac{\partial}{\partial x}\left(\frac{\partial}{\partial z} - \cot\alpha \frac{\partial}{\partial x}\right)\rho', \tag{9}$$

where $\beta = g\gamma\sin\alpha$. Using the transformation $\zeta = x - \frac{1}{2}\beta z t^2$, $\eta = z$, $\tau = t/\beta^{\frac{1}{2}}$ (see also Phillips (1966, p. 180) and Hartman (1975) for a similar transformation, but of a steady flow), we find

$$\frac{\partial}{\partial\tau}\left\{\frac{\partial}{\partial\tau}\left[\frac{\partial^2}{\partial\zeta^2} + \left(\frac{\partial}{\partial\eta} - \frac{\tau^2}{2}\frac{\partial}{\partial\zeta}\right)^2\right] + 2\tau\frac{\partial}{\partial\zeta}\left(\frac{\partial}{\partial\eta} - \frac{\tau^2}{2}\frac{\partial}{\partial\zeta}\right)\right\}\rho' + \cot\alpha\frac{\partial^2}{\partial\zeta^2}\rho' - \frac{\partial}{\partial\zeta}\left(\frac{\partial}{\partial\eta} - \frac{\tau^2}{2}\frac{\partial}{\partial\zeta}\right)\rho' = 0. \tag{10}$$

A solution which corresponds to a plane internal gravity wave at $t = 0$ is

$$\rho' = \rho(\tau)\exp i(k\zeta + l\eta),$$

where

$$\frac{d}{d\tau}\left\{k^2 + \left(l - \frac{\tau^2 k}{2}\right)^2\right\}\frac{d\rho}{d\tau} + \left\{k^2\cot\alpha - k\left(l - \frac{\tau^2 k}{2}\right)\right\}\rho = 0. \tag{11}$$

This may be rewritten in the form

$$d^2\phi/d\tau^2 + F(\tau)\,\phi = 0, \tag{12}$$

where

$$\phi(\tau) = [1 + (\lambda - \tfrac{1}{2}\tau^2)^2]^{\frac{1}{2}}\rho, \quad \lambda = l/k$$

and

$$F(\tau) = \frac{\cot\alpha\,[\tau^4 - 4\tau^2(\lambda + \tan\alpha) + 4(1+\lambda^2)]}{4[1 + (\lambda - \tfrac{1}{2}\tau^2)^2]^2}.$$

Growing solutions for ϕ will occur if $F(\tau) < 0$, i.e. when

$$2\{(\lambda+\tan\alpha)-(\tan^2\alpha+2\lambda\tan\alpha-1)^{\frac{1}{2}}\} < \tau^2 < 2\{(\lambda+\tan\alpha)+(\tan^2\alpha+2\lambda\tan\alpha-1)^{\frac{1}{2}}\}.$$

The smallest value of τ at which $F(\tau)$ becomes negative is $\tau^2 = \cot\alpha$ when $\lambda = \frac{1}{2}\cot\alpha$. (Here, however, $\rho = \rho(\tau)\exp i(kx+lz-\frac{1}{2}\beta zt^2k) = \rho(\tau)\exp ikx$ and the waves are of large vertical extent.) The time for which a wave with given (k, l) will grow is however restricted, and whilst limited growth may occur it will not be continued. At large τ the growth rate will in any case be restricted since $F \sim \cot\alpha/4\tau^2$ and $\rho \sim 2\phi/\tau^2$. It thus appears that waves of scale much less than the tube dimensions will not grow indefinitely and become unstable in a classical sense.

REFERENCES

Banks, W. H. H., Drazin, P. G. & Zaturska, M. B. 1976 On the normal modes of parallel flow of inviscid stratified fluid. *J. Fluid Mech.* **75**, 149–171.

Davey, A. & Reid, W. H. 1977 On the stability of stratified viscous plane Couette flow. Part 1. Constant buoyancy frequency. *J. Fluid Mech.* **80**, 509–526.

Eliassen, A., Høiland, E. & Riis, E. 1953 Two-dimensional perturbation of a flow with constant shear of a stratified fluid. *Inst. Weather Climate Res., Norwegian Acad. Sci. Lett. Publ.* no. 1.

Goodman, J. K. & Miller, A. 1977 Mass transport across a density inversion. *J. Geophys. Res.* **82**, 3463–3471.

Halpern, D. 1974 Observations of the deepening of the wind mixed layer in the Northeast Pacific Ocean. *J. Phys. Ocean.* **4**, 454–466.

Hartman, R. J. 1975 Wave propagation in a stratified shear flow. *J. Fluid Mech.* **71**, 89–104.

Holton, J. R. & Lindzen, R. S. 1972 An updated theory for the quasi-biennial oscillation of the tropical stratosphere. *J. Atmos. Sci.* **29**, 1076–1080.

Kato, H. & Phillips, O. M. 1969 On the penetration of a turbulent layer into stratified fluid. *J. Fluid Mech.* **37**, 643–655.

McEwan, A. D. & Robinson, R. M. 1975 Parametric instability of internal gravity waves. *J. Fluid Mech.* **67**, 667–688.

Phillips, O. M. 1966 *The Dynamics of the Upper Ocean.* Cambridge University Press.

Plumb, R. A. 1977 The interaction of two internal waves with the mean flow; implications for the theory of the quasi-biennial oscillation. *J. Atmos. Sci.* **34**, 1847–1858.

Scorer, R. S. & Wilson, S. D. R. 1963 Secondary instability in steady gravity waves. *Quart. J. Roy. Met. Soc.* **89**, 532–539.

Thorpe, S. A. 1968*a* On the shape of progressive internal waves. *Phil. Trans. Roy. Soc.* A **263**, 563–614.

Thorpe, S. A. 1968*b* A method of producing a shear flow in a stratified fluid. *J. Fluid Mech.* **32**, 693–704.

Thorpe, S. A. 1973 Experiments on instability and turbulence in a stratified shear flow. *J. Fluid Mech.* **61**, 731–751.

Thorpe, S. A. 1978*a* On the shape and breaking of finite amplitude internal gravity waves in a shear flow. *J. Fluid Mech.* **85**, 7–31.

Thorpe, S. A. 1978*b* The near-surface ocean mixing layer in stable heating conditions. *J. Geophys. Res.* **83**, 2875–2885.

Turner, J. S. 1973 *Buoyancy Effects in Fluids.* Cambridge University Press.

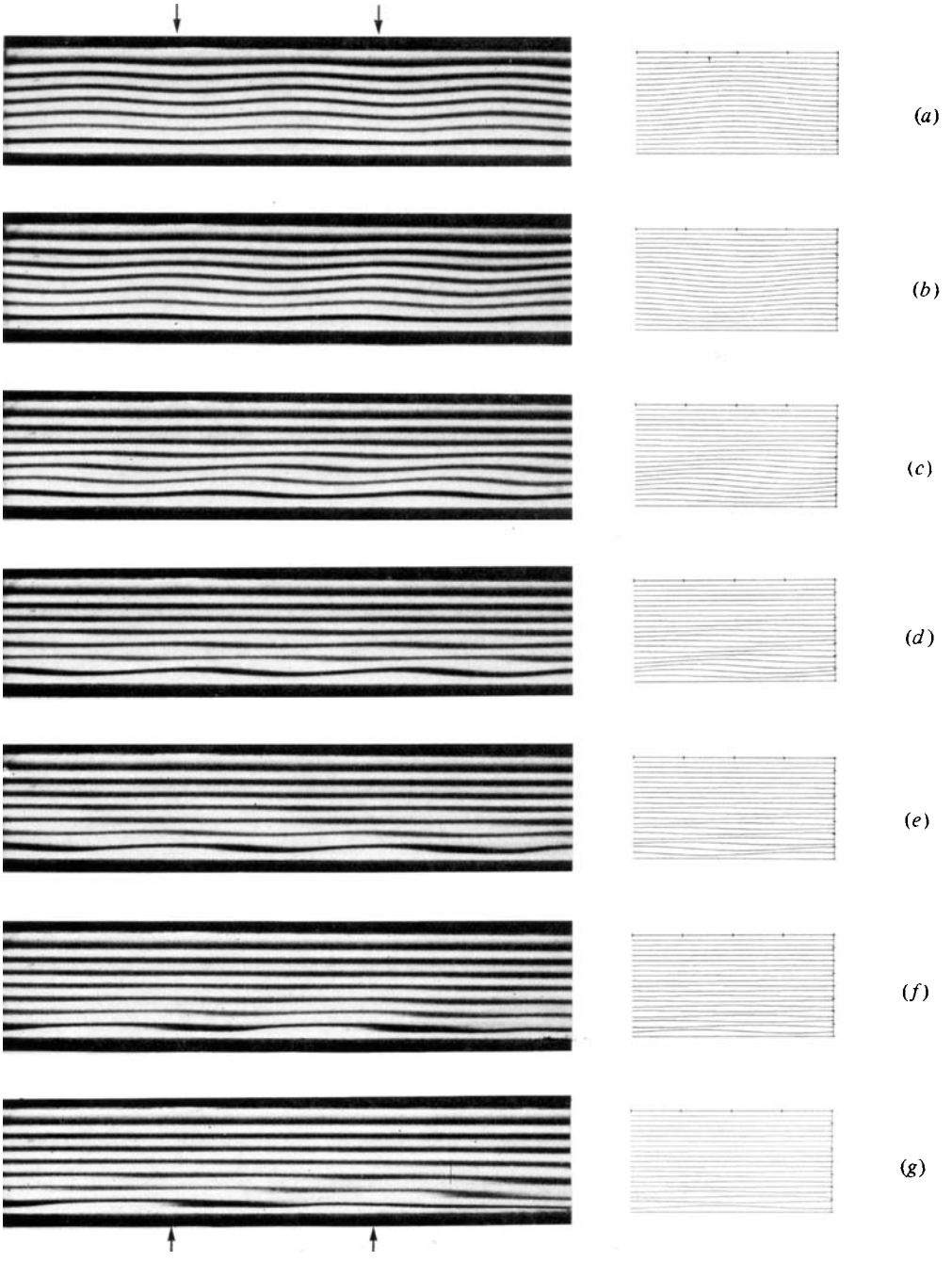

FIGURE 5. Experiment *A*. Waves of the first internal mode in an accelerating shear flow with a constant Brunt–Väisälä frequency $N = 2{\cdot}24$ rad s^{-1}. To the left are photographs of the flow in the tube, which is 16 cm in depth. The waves are propagating to the left and initially have a period 3·98 s. The photographs are at (*a*) $-0{\cdot}2$ s, (*b*) 2·1 s, (*c*) 3·85 s, (*d*) 6·2 s, (*e*) 8·0 s, (*f*) 9·8 s and (*g*) 11·3 s after the tube is tilted through 0·072 rad down to the left. The surge originating from the right end of the tube is seen entering the section in (*g*). To the right are shown computer simulations of lines of constant density (*a*) at the moment of tilt and (*b*)–(*g*) at subsequent 2 s intervals (see § 4).

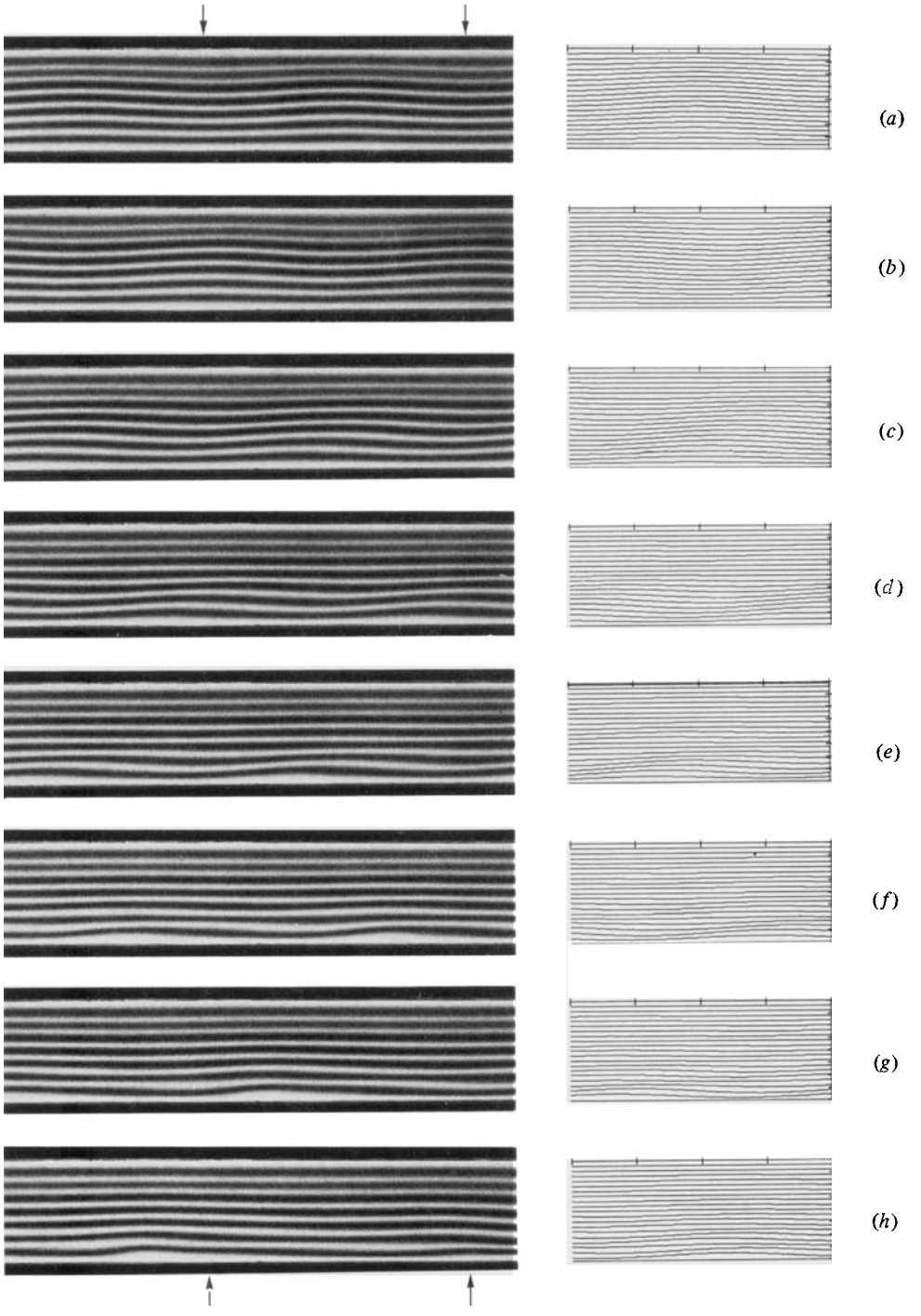

FIGURE 6. Experiment *B*. Waves of the first internal mode in an accelerating shear flow with a Brunt–Väisälä frequency $N = 2{\cdot}18$ rad s^{-1}. To the left are photographs of the flow in the tube, which is 16 cm in depth. The waves are propagating to the left and initially have a period 4·82 s. The tube was tilted at time $t = 0$ through 0·051 rad down to the left and back into a horizontal, position at 5·5 s. The photographs are at (*a*) −0·65 s, (*b*) 1·85 s, (*c*) 4·20 s, (*d*) 5·98 s, (*e*) 7·80 s, (*f*) 10·07 s, (*g*) 11·97 s and (*h*) 13·78 s. To the right are shown computer simulations of lines of constant density (*a*) at the moment of tilt and (*b*)–(*h*) at subsequent 2 s intervals (see § 4).

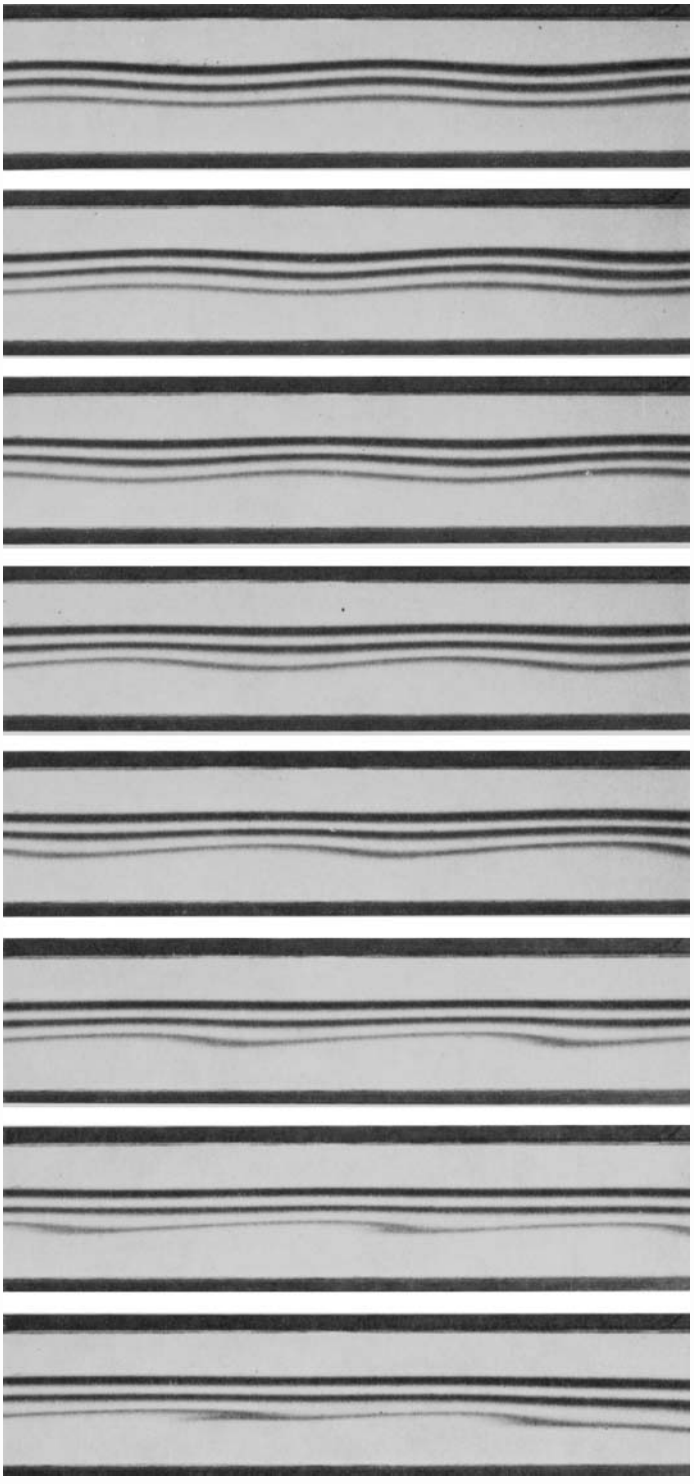

FIGURE 7. Experiment *C*. Waves of the first internal mode in an accelerating shear flow with uniform density in layers 5·75 cm thick above and below the upper and lower dye lines respectively and an approximately constant Brunt–Väisälä frequency $N = 5{\cdot}05$ rad s^{-1} between. The tube depth is 16 cm. The waves propagate to the left and initially have a period 2·75 s. The waves are shown at (*a*) −0·13 s, (*b*) 1·78 s, (*c*) 3·22 s, (*d*) 4·67 s, (*e*) 6·10 s, (*f*) 7·07 s, (*g*) 8·05 s and (*h*) 9·00 s after the tube was tilted down to the left through 0·041 rad. The surge originating from the right-hand end of the tube is seen entering the section in (*h*).